

Research article

Sunlight-driven degradation of chlorpyrifos and imidacloprid using TiO₂/PHEMA nanocomposite: Synthesis, characterization, and photocatalytic performance

Zarah Alqarni^{a,*}^aDepartment of Chemistry, College of Science, University of Jeddah, Jeddah 21589, Saudi Arabia

ARTICLE INFO

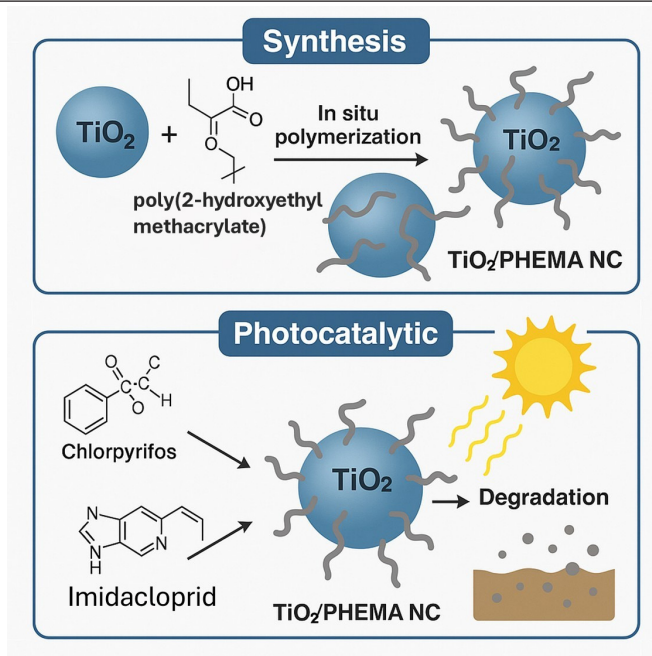
Keywords:

TiO₂/PHEMA nanocomposite
Photocatalytic degradation
Chlorpyrifos
Imidacloprid
Visible light
Pesticide removal
Band gap reduction

ABSTRACT

The environmental persistence and toxicity of chlorpyrifos (CPF) and imidacloprid (IMD) necessitate the development of efficient, solar-driven remediation strategies. This study reports the synthesis of a TiO₂/poly(2-hydroxyethyl methacrylate) nanocomposite (TiO₂/PHEMA NC) via in situ radical polymerization and evaluates its photocatalytic performance under natural sunlight. Comprehensive characterization (ultraviolet–visible spectroscopy (UV–Vis), Fourier transform infrared spectroscopy (FTIR), X-ray diffraction (XRD), transmission electron microscopy (TEM), thermogravimetric analysis (TGA)) confirms the successful incorporation of TiO₂ into the polymer matrix, resulting in a narrowed band gap (~2.6 eV), improved dispersion, and enhanced interfacial charge transfer. Photocatalytic tests demonstrate significantly higher degradation efficiencies of CPF (95.6%) and IMD (97.3%) by TiO₂/PHEMA compared to pristine TiO₂, with superior reaction kinetics ($k \approx 0.019 \text{ min}^{-1}$) and recyclability over five cycles. The enhanced activity is attributed to synergistic effects, including bandgap modulation, reduced recombination, and improved surface accessibility. This work provides the first evidence of TiO₂/PHEMA application for dual pesticide degradation under solar irradiation, highlighting its promise as a scalable and sustainable photocatalyst for environmental purification.

GRAPHICAL ABSTRACT



*Corresponding author:

E-mail address: zhal-qarni@uj.edu.sa (Z.H. Alqarni)

Received: 29 August, 2025 Accepted: 08 November, 2025 Epub Ahead of Print: 09 February, 2026 Published: 24 February, 2026

DOI: 10.25259/JKSUS_1370_2025

1. Introduction

The widespread use of pesticides in contemporary agriculture has led to the persistent contamination of aquatic environments, posing serious risks to ecosystems and human health (Zhou *et al.*, 2025). Among the most hazardous compounds are chlorpyrifos (CPF), a widely applied organophosphate insecticide, and imidacloprid (IMD), a neonicotinoid used extensively for crop protection (Motaung, 2020, Nandhini *et al.*, 2021). CPF exhibits strong hydrophobicity, low biodegradability, and a high affinity for organic matter, leading to long-term persistence and bioaccumulation in water bodies (Kumar *et al.*, 2023). IMD, although more water-soluble, is similarly resistant to natural degradation and is linked to neurotoxicity in non-target organisms. Both compounds are toxic even at low concentrations and have been frequently detected in surface and groundwater (Yoloğlu *et al.*, 2025). Conventional treatment approaches such as adsorption (Cosgrove *et al.*, 2019), coagulation-flocculation (Narayanan *et al.*, 2020), biological degradation (Conde-Avila *et al.*, 2021), and advanced oxidation processes have been employed but often suffer from incomplete mineralization, high energy demands, or secondary pollution (Leskovic and Petrović 2023). These limitations highlight the need for efficient, sustainable, and solar-driven degradation strategies to remove recalcitrant pesticides from contaminated water.

Semiconductor-based photocatalysis has emerged as a promising approach for degrading persistent organic pollutants in water (Wu *et al.*, 2023, Nezzal *et al.*, 2025). In particular, titanium dioxide (TiO₂) has been extensively investigated due to its high chemical stability, low toxicity, and strong oxidative potential under UV irradiation (Racovita 2022, Ghamarpoor *et al.*, 2023). For example, Shorgoli and Shokri (2017) demonstrated nearly 90% removal of IMD using TiO₂ immobilized on glass under UV light (Akbari Shorgoli and Shokri 2017), while Saljooqi *et al.* (2020) reported more than 94% degradation of CPF with a ZnO/TiO₂-Fe₃O₄ nanocomposite (NC) under optimized conditions (Saljooqi *et al.*, 2021). Despite such promising results, the photocatalytic performance of pristine TiO₂ is fundamentally restricted by its relatively wide band gap (~3.2 eV for anatase), which confines activation to the ultraviolet region, representing less than 5% of the solar spectrum, and by the rapid recombination of photoinduced charge carriers, which drastically lowers the yield of reactive oxygen species (Nekooie *et al.*, 2021, Althamthami *et al.*, 2023a). These intrinsic drawbacks have limited the practical efficiency of TiO₂ under natural sunlight, motivating extensive research into modification strategies to expand visible-light utilization and enhance charge-carrier dynamics.

To overcome the inherent drawbacks of pristine TiO₂, including its wide band gap and rapid charge-carrier recombination, several modification strategies have been developed (Althamthami *et al.*, 2023b). Approaches such as metal or nonmetal doping, heterojunction formation with narrow-band-gap semiconductors, and noble-metal decoration have been widely explored to extend light absorption and enhance charge separation (Kumar *et al.*, 2022). More recently, polymer hybridization has emerged as an attractive alternative, where organic polymers provide a conductive or functional matrix that improves nanoparticle (NP) dispersion, increases interfacial contact, and facilitates electron transport. For example, Nekooie *et al.* reported that CuO/TiO₂/PANI NC degraded 95% of CPF under visible light within 90 min, outperforming pristine TiO₂ and binary composites due to efficient interfacial charge transfer (Nekooie *et al.*, 2021). Similarly, molecularly imprinted polymers (MIPs) have been used to couple with semiconductors such as CdS quantum dots, achieving selective recognition and photodegradation of IMD and bupropion with efficiencies above 80% (Malik *et al.*, 2023). These findings demonstrate that polymer modification not only enhances solar-light harvesting but also improves adsorption capacity and catalytic selectivity.

In this context, poly(2-hydroxyethyl methacrylate) (PHEMA) is an appealing polymer support for TiO₂ due to its hydrophilicity and abundant hydroxyl and carbonyl groups, which interact strongly with TiO₂ surfaces. Such interactions stabilize TiO₂ NPs, prevent agglomeration, and promote interfacial charge transfer, thereby reducing recombination and extending light absorption into the visible region (Alamgir *et al.*, 2021b, 2022). Moreover, the amorphous PHEMA network can confine crystallite growth, ensure uniform dispersion,

and provide mechanical robustness, all of which are critical for photocatalyst durability and recyclability (Ussia *et al.*, 2018). Previous studies on PHEMA-TiO₂ composites, however, have mainly focused on non-environmental applications. Moradi *et al.* developed GO/HEMA and GO/HEMA/TiO₂ NC for dye adsorption, reporting effective removal of methylene blue and methyl orange (Moradi *et al.*, 2021). Alamgir and co-workers fabricated PHEMA/TiO₂ and PHEMA /TiO₂/GO by melt processing, improving thermomechanical and dental properties (Alamgir *et al.*, 2021b). Erol *et al.* synthesized PHEMA/TiO₂ via in situ polymerization/hydrothermal methods and investigated their thermal, swelling, dielectric, and antibacterial properties (Erol *et al.*, 2022). While these studies demonstrated that PHEMA stabilizes TiO₂ and improves interfacial properties, none evaluated pesticide degradation under sunlight. Therefore, TiO₂/PHEMA NC represents a multifunctional platform that integrates enhanced optical properties, efficient charge dynamics, and structural stability, offering a sustainable and scalable solution for pesticide remediation in aqueous environments.

While TiO₂-based NCs have been widely investigated for the removal of dyes, antibiotics, and other pharmaceuticals, their use in the simultaneous degradation of organophosphate and neonicotinoid pesticides under natural sunlight remains largely unexplored. Previous studies on polymer-TiO₂ systems, including PHEMA/TiO₂ hybrids, have mainly addressed thermal, dielectric, or biomedical properties rather than environmental applications (Alamgir *et al.*, 2021b, 2022; Erol *et al.*, 2022). Reports on polymer-semiconductor photocatalysts often target single pollutant classes under artificial light and lack mechanistic insight. Given the persistence and distinct degradation challenges of CPF and IMD, exploring their concurrent removal under solar irradiation highlights a critical gap. It underscores the potential of polymer matrices to enhance visible-light-driven photocatalysis for multifunctional pesticide remediation.

This study presents the synthesis of a TiO₂/PHEMA NC via in situ polymerization and its application in the photocatalytic degradation of CPF and IMD under direct sunlight. To the best of our knowledge, this is the first report on TiO₂/PHEMA for pesticide remediation, extending the utility of this hybrid beyond biomedical and dielectric applications into environmental purification. The NC demonstrated a narrowed band gap, enhanced charge separation, and superior stability, achieving markedly higher degradation efficiencies than pristine TiO₂. Comprehensive characterization (ultraviolet-visible spectroscopy (UV-Vis), Fourier transform infrared spectroscopy (FTIR), X-ray diffraction (XRD), transmission electron microscopy (TEM), thermogravimetric analysis (TGA)) and photocatalytic assessments elucidated the mechanism and underscored the critical role of polymer-semiconductor interactions. These findings establish TiO₂/PHEMA as a novel, sunlight-responsive, and recyclable platform for sustainable pesticide remediation in aqueous environments.

2. Materials and Methods

2.1. Materials

Titanium(IV) isopropoxide (Ti[OCH(CH₃)₂]₄, 99.99%), 2-hydroxyethyl methacrylate (HEMA) (CH₂=C(CH₃)COOCH₂CH₂OH, 99%), ammonium persulfate ((NH₄)₂S₂O₈, 98%), isopropyl alcohol ((CH₃)₂CHOH, ≥99.5%), glacial acetic acid (CH₃CO₂H, 99.7%), and hydrochloric acid (HCl, 37%) were purchased from Sigma-Aldrich and used as received without further purification. All solvents were of analytical grade. CPF (C₉H₁₁Cl₂NO₃PS, ≥98%) and IMD (C₉H₁₀ClN₅O₂, analytical standard, ≥98%) were obtained from Merck and used as model pollutants for photocatalytic degradation studies. All experiments involving CPF, IMD, and solvents were conducted in accordance with institutional safety protocols. Pesticide residues and solvent wastes were collected in designated containers and disposed of through the university's hazardous waste management system.

2.2. Synthesis of TiO₂ NPs

TiO₂ NPs were synthesized via a modified solvothermal route adapted from established protocols (Ramakrishnan *et al.*, 2020). In a typical preparation, 0.08 mol of Ti[OCH(CH₃)₂]₄ was dissolved in 100

mL of 1 M isopropanol and stirred on a hot plate at 70°C for 12 min to obtain a homogeneous solution. Subsequently, 12 mL of glacial acetic acid was introduced dropwise under continuous stirring, and the reaction mixture was maintained at the same temperature for an additional 3 h to promote controlled hydrolysis and condensation of the titanium precursor. The resulting sol was transferred into a 400 mL Teflon-lined stainless-steel autoclave and subjected to solvothermal treatment at 170°C for 7 h. After cooling to room temperature, the precipitate was collected by centrifugation, repeatedly washed with distilled water and ethanol to remove unreacted species and residual organics, and then dried at 60°C for 7 h. Finally, the dried powder was annealed at 450°C for 2 h in air to enhance crystallinity and phase stability of the TiO₂ NPs.

2.3. Synthesis of TiO₂/PHEMA NC

TiO₂/PHEMA NC was synthesized through a one-pot in situ radical polymerization method adapted from reported procedures (Erol *et al.*, 2022). In a typical preparation, 100 mg of TiO₂ NPs were dispersed in 10 mL of 1.0 M hydrochloric acid containing 0.2 mL of 2-hydroxyethyl methacrylate (HEMA) monomer. The dispersion was sonicated for 25 min to achieve uniform distribution of TiO₂ within the monomeric solution. Subsequently, 5 mL of 1.0 M HCl solution containing 0.5 g of ammonium persulfate (APS) as a free-radical initiator (molar ratio 1:1 with respect to HEMA) was introduced dropwise under constant stirring. The mixture was maintained at 55°C with vigorous agitation for 4 h, allowing complete polymerization and simultaneous incorporation of TiO₂ into the poly(2-hydroxyethyl methacrylate) matrix. After the reaction, the obtained TiO₂/PHEMA NC was separated by filtration, thoroughly washed with ethanol and deionized water to remove unreacted monomers and initiator residues, and dried at 55°C for 12 h. The dried material was then finely ground using an agate mortar to obtain a homogeneous powder for subsequent characterization. For comparison, pure PHEMA was synthesized following the same protocol in the absence of TiO₂ NPs.

2.4. Characterization

Various analytical techniques were employed to investigate the physicochemical properties of the synthesized TiO₂ NPs and TiO₂/PHEMA NC. FTIR spectroscopy was performed using a Bruker Tensor II spectrometer (Bruker Corporation, Germany) to identify functional groups and confirm the successful polymerization of HEMA and its interaction with TiO₂. The crystalline structure and phase composition were analyzed by XRD using a PANalytical X'Pert PRO diffractometer (Malvern PANalytical, Netherlands) with CuK α radiation ($\lambda = 0.15418$ nm) (Salmi *et al.*, 2024).

$$D = \frac{K\lambda}{\beta \cos\theta} \quad (1)$$

The average crystallite size (D) was calculated using the Debye-Scherrer equation, where K is the shape factor (0.9), β is the full width at half maximum (FWHM), and θ is the Bragg angle. Morphological features and particle dispersion were examined by TEM using a JEOL JEM-2100 microscope (JEOL Ltd., Japan). Thermal stability and decomposition behavior were assessed via TGA using a Q500 analyzer (TA Instruments, USA) under a nitrogen atmosphere. UV-visible spectroscopy in the 200–800 nm range was carried out using a Shimadzu UV-2600 spectrophotometer (Shimadzu Corporation, Japan) to determine optical absorption and estimate the band gap energy.

2.5. Photocatalytic activity

The photocatalytic activity of the synthesized TiO₂ NPs and TiO₂/PHEMA NC was evaluated for the degradation of CPF and IMD under natural sunlight irradiation. Experiments were conducted in April 2025 in Jeddah, Saudi Arabia (21.49°N, 39.19°E) under clear-sky conditions, with an average solar irradiance of 650–780 W m⁻² (measured by a calibrated pyranometer, Kipp & Zonen) between 10:00 AM and 2:00 PM, and an ambient temperature ranging from 28–32°C. The spectral distribution was referenced against ASTM G-173 standard solar spectra,

and photon flux was verified by potassium ferrioxalate actinometry, yielding $\sim 4.2 \times 10^5$ mol photons m⁻² s⁻¹ in the 300–400 nm region. Stock pesticide solutions of CPF and IMD were freshly prepared at a concentration of 5 mg L⁻¹ in a total volume of 200 mL. Aliquots were withdrawn from these stock solutions and used for each photocatalytic run. In a typical experiment, 5 mg of photocatalyst was dispersed in 10 mL of pesticide solution (5 mg L⁻¹, pH 10) and irradiated with sunlight for 10–90 min. Before light exposure, all suspensions were magnetically stirred in the dark for 20 min to establish adsorption-desorption equilibrium. Control experiments confirmed that no significant degradation occurred in the dark, indicating that pesticide removal was solely driven by photocatalysis.

The influence of operational parameters was systematically studied. The effect of pH was examined over the range 4–10 by adjusting the solution with 0.1 M HCl or NaOH, while maintaining an initial concentration of 5 mg L⁻¹, a catalyst dosage of 5 mg, and 90 min of irradiation. The role of initial pesticide concentration was assessed by varying levels between 5 and 15 mg L⁻¹ at pH 7 with 5 mg catalyst and 90 min irradiation. Catalyst loading was investigated by dispersing 20–50 mg in 10 mL of pesticide solution (5 mg L⁻¹, pH 10) and irradiating for 90 min.

At predetermined intervals, aliquots were collected, centrifuged to remove catalyst particles, and analyzed using a UV-Vis spectrophotometer at $\lambda_{max} = 245$ nm for CPF and 270 nm for IMD. The photocatalytic degradation efficiency (%) was calculated according to Eq. (2) (Salmi *et al.*, 2023):

$$\% \text{degradation} = \frac{C_0 - C_t}{C_0} \times 100 \quad (2)$$

Where C_0 and C_t represent the initial concentration and the concentration at irradiation time t , respectively.

2.6. Reusability experiment

The reusability of the TiO₂/PHEMA NC photocatalyst was evaluated through consecutive degradation cycles of CPF and IMD under natural sunlight irradiation. After each photocatalytic run, the catalyst was recovered by centrifugation, washed thoroughly with deionized water and ethanol to remove residual pollutants, and dried at 60°C for 6 h before being reused in the subsequent cycle. This procedure was repeated for five consecutive runs under identical experimental conditions (5 mg L⁻¹ pesticide solution, 5 mg catalyst dosage, pH 10, and 90 min irradiation time). The degradation efficiency was calculated at the end of each cycle to assess the photocatalyst's stability and recyclability.

3. Results and Discussion

3.1. UV-Vis spectroscopy and band gap analysis

The optical absorption spectra of TiO₂ NPs and the TiO₂/PHEMA NC display well-defined edges in the near-UV region, characteristic of intrinsic band-to-band transitions in TiO₂. For pristine NPs, the absorption onset occurs around 348 nm, whereas incorporation of PHEMA results in a slight bathochromic shift to 358 nm (Fig. 1a, Table 1). This redshift indicates that the polymer matrix modifies the local electronic environment of TiO₂, likely through interfacial interactions between hydroxyl or carbonyl groups of PHEMA and surface Ti sites. Such interactions can introduce shallow defect states, promote interfacial charge transfer, and reduce agglomeration, thereby extending the absorption profile marginally into the visible region (Rahimli and Musayeva 2025). The optical band gap energy (E_g) was estimated by plotting $(\alpha h\nu)^2$ versus photon energy (Tauc plot) and extrapolating the linear region (Johannes *et al.*, 2020). Tauc plot analysis corroborates this observation, revealing a bandgap energy of ~ 2.65 eV for the TiO₂/PHEMA NC, which is significantly lower than that of pristine TiO₂ NPs (Fig. 1b). This narrowing of the bandgap can be attributed to defect-mediated electronic states and enhanced polymer-semiconductor coupling, which reduce the excitation threshold for electron-hole

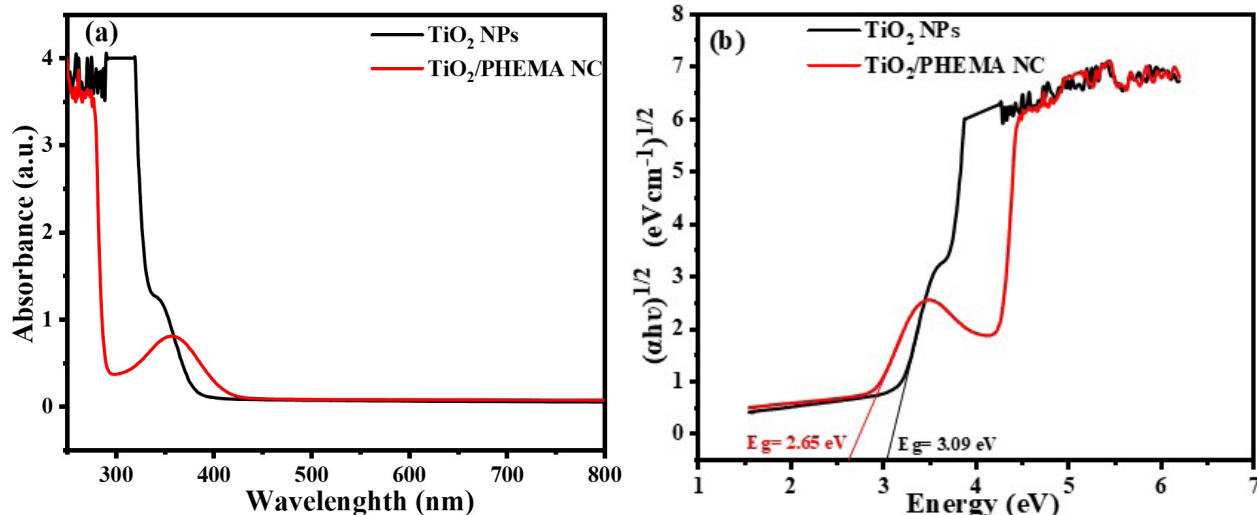


Fig. 1. UV-Vis absorption spectra of bandgap energy of (a) TiO₂ NPs and (b) TiO₂/PHEMA NC.

Table 1.
Optical absorption peak and band gap energy of TiO₂ and TiO₂/PHEMA NC.

Sample	Absorption peak (nm)	Band gap energy (eV)
TiO ₂ NPs	348	3.09
TiO ₂ /PHEMA NC	358	2.65

generation. In comparison, bulk anatase TiO₂ typically exhibits a bandgap of ~3.2 eV, and sol-gel or hydrothermally derived NPs generally fall within the range of 3.1–3.3 eV (Shejale et al., 2021). The observed reduction, therefore highlights the effectiveness of PHEMA incorporation in tailoring the optical properties of TiO₂, enabling improved utilization of solar light for photocatalytic processes.

3.2. FTIR analysis

The FTIR spectra of PHEMA, TiO₂ NPs, and TiO₂/PHEMA NC confirm the structural features of each component and their effective integration in the NC (Fig. 2). For PHEMA, the broad absorption band at 3444 cm⁻¹ corresponds to O–H stretching vibrations, while the peak at 2924 cm⁻¹ is due to aliphatic C–H stretching (Makreski et al., 2018; Boral et al., 2021). The band at 1614 cm⁻¹ is attributed to skeletal

vibrations of C=C bonds, likely originating from residual vinyl groups or the polymer backbone (Nahas et al., 2025). Additional peaks at 1345 cm⁻¹ and 1079 cm⁻¹ are assigned to C–H bending and C–O–C stretching of ester groups, respectively (Ma et al., 2016, Toledo et al., 2018, Zhang and Sun 2020), whereas the band at 623 cm⁻¹ corresponds to C–H out-of-plane bending. In the spectrum of TiO₂ NPs, the broad signal near 3444 cm⁻¹ indicates surface hydroxyl groups and adsorbed water, while the peak at 1459 cm⁻¹ corresponds to C–H bending vibrations (Gopanna et al., 2019). The characteristic Ti–O–Ti stretching modes are observed at 623, 549, and 438 cm⁻¹, confirming the formation of TiO₂ (Moradi et al., 2021, Qutub et al., 2022). In the TiO₂/PHEMA NC spectrum, the coexistence of polymeric features (3444, 1614, 1079 cm⁻¹) alongside TiO₂ lattice vibrations (623, 549, 438 cm⁻¹) demonstrates successful incorporation of TiO₂ into the PHEMA matrix. The retention and slight shifts of these bands suggest interfacial interactions, such as hydrogen bonding between PHEMA functional groups and TiO₂ surface hydroxyls, confirming the formation of a stable hybrid NC.

3.3. XRD analysis

The XRD analysis provides clear insight into the structural features of the prepared materials (Fig. 3). Neat PHEMA exhibits a broad diffraction

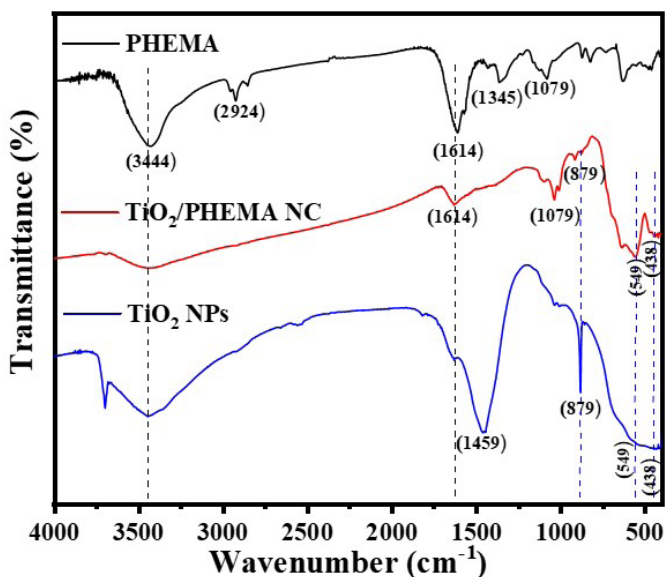


Fig. 2. FT-IR spectra of PHEMA, TiO₂ NPs, and TiO₂/PHEMA NC.

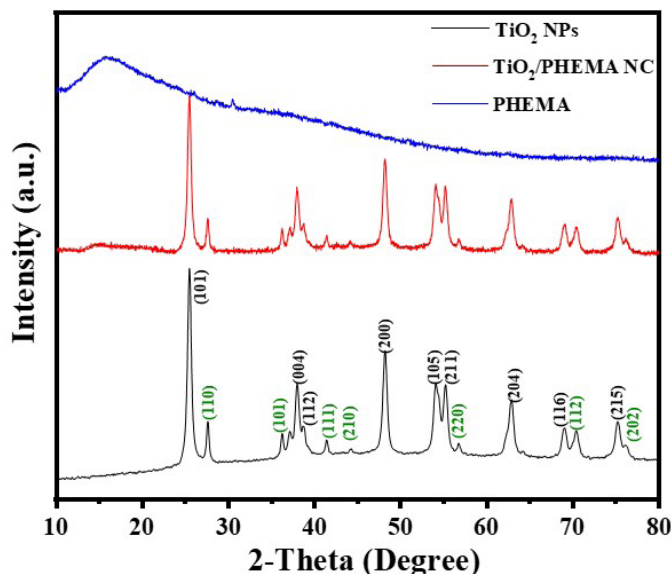


Fig. 3. XRD pattern of PHEMA, TiO₂ NPs and TiO₂/PHEMA NC.

peak at $2\theta \approx 13.82^\circ$, confirming its amorphous nature (Alamgir *et al.*, 2021a). In contrast, TiO_2 NPs display sharp reflections at $2\theta = 25.3^\circ$, 37.9° , 38.6° , 48.1° , 54.0° , 55.2° , 62.8° , 68.9° , and 75.2° , indexed to the (101), (004), (112), (200), (105), (211), (204), (116), and (215) planes of the anatase phase (JCPDS 01-073-1764), respectively. Additional peaks at 27.6° , 36.2° , 41.4° , 44.3° , 57.0° , 70.1° , and 76.9° correspond to the (110), (101), (111), (210), (220), (112), and (202) planes of the rutile phase, respectively (JCPDS 01-088-1172), confirming the coexistence of anatase and rutile polymorphs. The TiO_2 /PHEMA NC retains these crystalline reflections alongside the amorphous halo of the polymer, though with reduced intensities, indicating effective encapsulation and uniform dispersion of TiO_2 crystallites within the PHEMA matrix. For crystallite size determination, the most intense anatase (101) reflection at $2\theta = 25.3^\circ$ was employed, using a shape factor (K) of 0.9 and β corrected for instrumental broadening. Crystallite size calculations using the Scherrer equation revealed an average size of ~ 34 nm for pure TiO_2 , which slightly decreased to ~ 32.9 nm in the composite, suggesting that the polymer phase restricts crystal growth and suppresses agglomeration (Bokuniaevea and Vorokh 2019). Importantly, the coexistence of anatase and rutile phases is advantageous, as their heterojunctions promote efficient charge separation and electron transfer, enhancing photocatalytic efficiency. Simultaneously, the amorphous PHEMA network enhances NP stability and homogeneity, resulting in a structurally robust hybrid material with synergistic properties.

3.4. TGA analysis

TGA evaluated the thermal stability of TiO_2 NPs and TiO_2 /PHEMA NC in the range of 25–800°C (Fig. 4). Pure TiO_2 NPs exhibited excellent stability, showing only minor weight losses of 3.3% between 50–200°C, attributed to the evaporation of physically adsorbed moisture and surface hydroxyl groups (Lothenbach *et al.*, 2016), and an additional 3.9% loss up to 800°C, likely due to the gradual removal of residual organic species or lattice oxygen release. In contrast, the TiO_2 /PHEMA NC demonstrated a more pronounced multi-step degradation profile. An initial weight loss of 8.5% in the 50–160°C range corresponds to the removal of physically bound water and low-molecular-weight volatiles entrapped in the polymer network. The significant degradation, amounting to $\sim 33.9\%$ between 200–800°C, is attributed to the thermal decomposition of the PHEMA matrix, involving chain scission, depolymerization, and oxidative degradation of the organic backbone (Carboué *et al.*, 2022). Compared with neat TiO_2 , the higher weight loss of the NC reflects the presence of the organic polymer fraction, while the residual weight at 800°C confirms the stable inorganic TiO_2 framework. These results highlight the superior thermal stability of

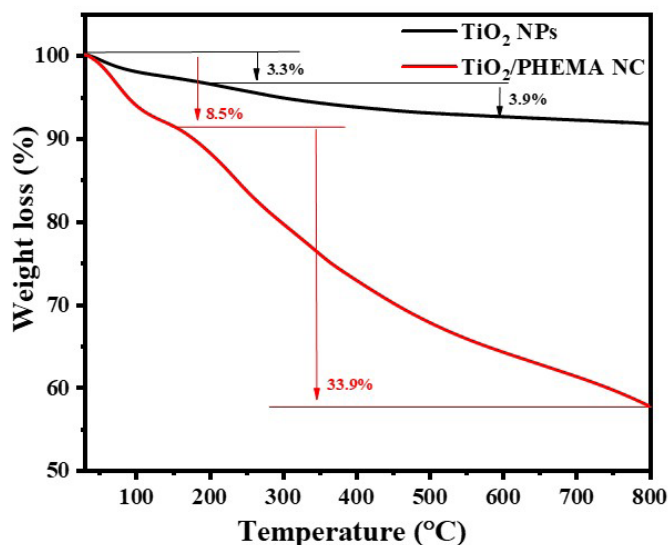


Fig. 4. TGA analysis of TiO_2 NPs and TiO_2 /PHEMA NC.

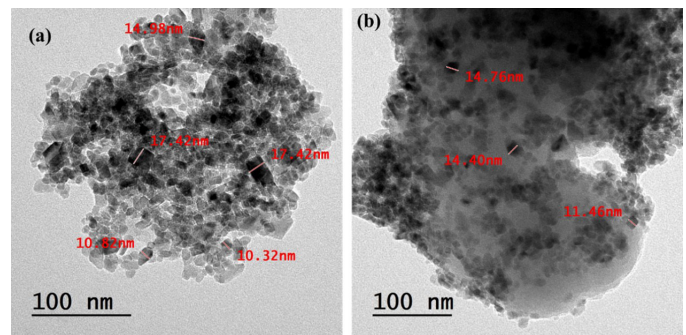


Fig. 5. TEM micrographs of (a) TiO_2 NPs and (b) TiO_2 /PHEMA NC.

TiO_2 NPs and the typical polymer-degradation behavior of PHEMA, and confirm the successful incorporation of TiO_2 into the polymer matrix.

3.5. TEM analysis

The TEM analysis provides detailed insight into the morphology and size distribution of the synthesized materials. For the pristine TiO_2 NPs (Fig. 5a), the images reveal quasi-spherical particles with a relatively uniform distribution and an average size of ~ 14.2 nm, forming loosely aggregated clusters. In contrast, the TiO_2 /PHEMA NC (Fig. 5b) exhibits NPs embedded within a lower-contrast amorphous matrix corresponding to the PHEMA phase. The incorporation of the polymer results in a slight reduction of the mean particle size to ~ 13.5 nm, along with a more diffuse morphology and diminished interparticle agglomeration, highlighting the role of PHEMA in restricting particle growth and stabilizing dispersion. The smaller particle size in the composite can be attributed to the polymer chains acting as a confining medium, limiting crystal coalescence during synthesis and subsequent thermal treatment (Tan *et al.*, 2016, Mohammed *et al.*, 2025). It should also be noted that while TEM provides direct visualization of particle diameters, XRD analysis reflects the coherent scattering domain size, which may differ due to microstrain, lattice defects, or instrumental factors. Nonetheless, the average particle sizes obtained from TEM align closely with the Scherrer-derived crystallite sizes (~ 34 nm for TiO_2 and ~ 32.9 nm for TiO_2 /PHEMA NC), thereby confirming the nanoscale dimensions of the materials and supporting the conclusion that the polymer matrix effectively moderates crystallite growth and maintains the structural integrity of the TiO_2 phase.

3.6. Degradation of CPF and IMD

The time-dependent photocatalytic degradation profiles of CPF and IMD (Figs. 6a-b) demonstrate a clear correlation between irradiation duration and removal efficiency. In both cases, a steady decline in the characteristic absorption peaks with prolonged exposure confirms the progressive mineralization of the pesticides. UV-visible spectrophotometric analysis identified the maximum absorption wavelength (λ_{max}) of CPF at 289 nm and IMD at 271 nm, which were used to monitor their degradation (Akbari Shorgoli and Shokri 2017, Adanan *et al.*, 2025). For TiO_2 NPs, degradation followed a gradual pathway, reaching 81% for CPF and 83.5% for IMD after 90 min. In contrast, the TiO_2 /PHEMA NC achieved markedly higher efficiencies, 95.6% for CPF and 97.3% for IMD, within the same irradiation period. The sharper decline observed during the initial 40–50 min reflects rapid generation of reactive oxygen species and effective electron-hole separation facilitated by the composite structure. Kinetic analysis was performed using the pseudo-first-order model expressed as (Khairan and Shrivastava 2019):

$$\ln(C_0 / C_t) = kt \quad (3)$$

Where C_0 and C_t represent the initial and residual concentrations of the pesticide at irradiation time t , and k is the apparent rate constant.

Kinetic analysis further confirmed the enhanced photocatalytic performance of the TiO_2 /PHEMA NC. The apparent rate constants for CPF (0.0336 min^{-1}) and IMD (0.0377 min^{-1}) were nearly double those

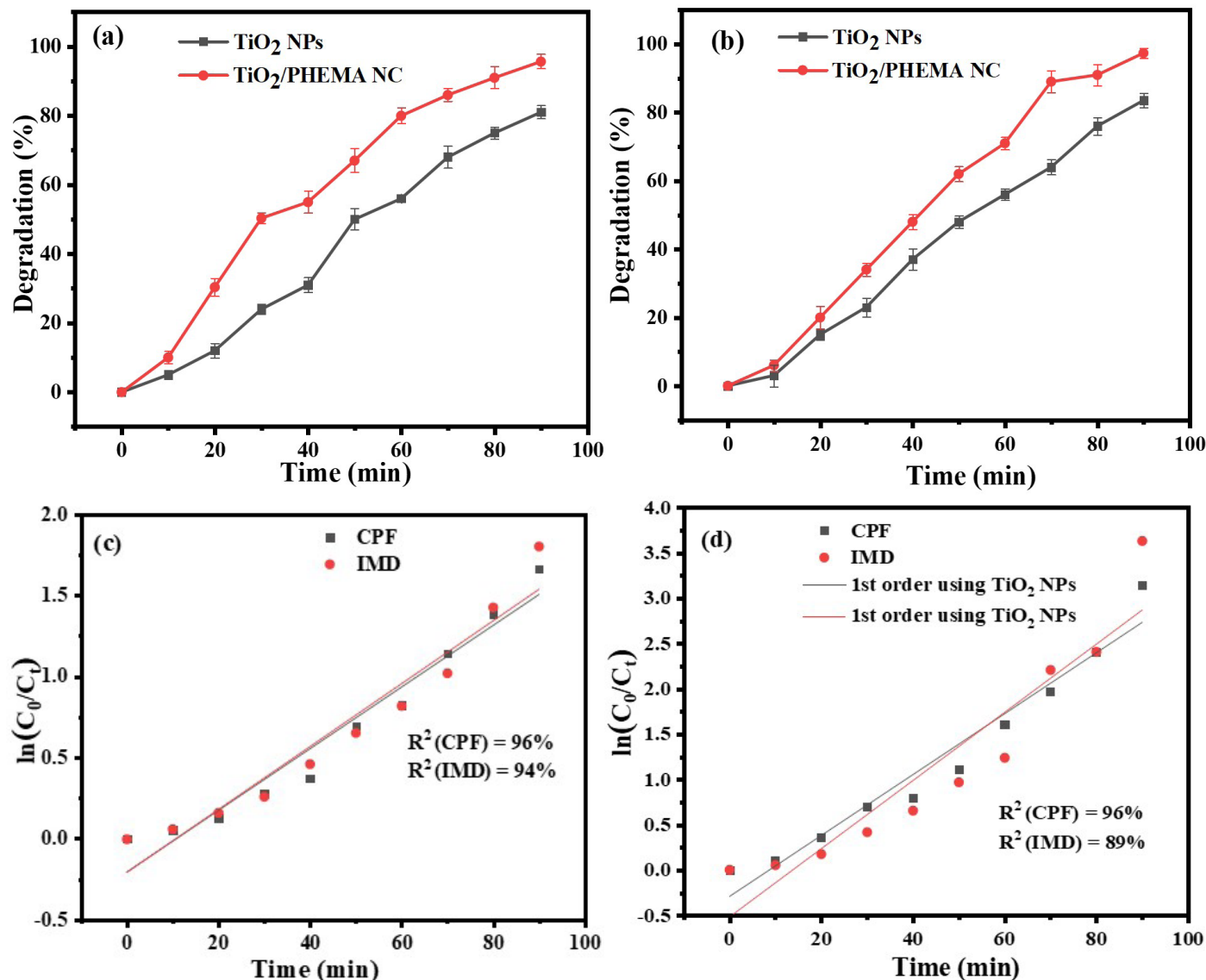


Fig. 6. UV-Vis spectra and photocatalytic degradation of (a) CPF and (b) IMD using TiO₂ NPs and TiO₂/PHEMA NC; First-order kinetic plot of $\ln(A_0/A_t)$ versus time of (c) TiO₂ NPs, and (d) TiO₂/PHEMA NC.

Table 2.

Photocatalytic degradation performance of CPF and IMD using TiO₂ NPs and TiO₂/PHEMA NC.

Photocatalyst	Pesticide	Degradation (%)	k (min ⁻¹)	R ² (%)
TiO ₂ NPs	CPF	81.0 ± 1.9	0.0190	96
	IMD	83.5 ± 2.1	0.0194	94
TiO ₂ /PHEMA NC	CPF	95.6 ± 2.2	0.0336	96
	IMD	97.3 ± 1.5	0.0377	89

of pristine TiO₂ (0.0190 and 0.0194 min⁻¹, respectively), demonstrating significantly accelerated degradation dynamics under sunlight (Fig. 6c and d, Table 2). The consistently higher *k* values of the NC indicate improved charge-separation efficiency and stronger responsiveness to solar irradiation compared with unmodified TiO₂. The enhanced activity of the NC can be attributed to several synergistic effects: the PHEMA matrix improves NP dispersion and suppresses agglomeration, increases photon absorption through a slight redshift in the absorption edge, and establishes interfacial charge-transfer pathways that minimize electron-hole recombination (Tiwari and Dhoble 2016). These effects were confirmed by characterization, where TEM revealed improved dispersion and reduced aggregation, UV-Vis analysis demonstrated

an extended absorption edge; FTIR indicated interfacial interactions between PHEMA functional groups and TiO₂ surface sites, and XRD showed restricted crystallite growth. These combined structural and electronic modifications imparted by the polymer support result in enhanced photon utilization, prolonged carrier lifetimes, and a higher density of active surface sites, thereby enabling the TiO₂/PHEMA NC to achieve significantly greater pesticide mineralization efficiency under identical irradiation conditions. A comparative evaluation (Table 3) further confirms that the TiO₂/PHEMA NC achieves superior degradation efficiency under sunlight, outperforming pristine TiO₂, and demonstrating strong potential as an effective photocatalyst for pesticide removal.

3.7. Effect of various parameters on photocatalytic activity

3.7.1. Effect of pH

The effect of pH on the photocatalytic performance of the TiO₂/PHEMA NC toward CPF and IMD (Fig. 7). Both pesticides displayed enhanced degradation efficiencies as the pH increased from acidic to alkaline conditions. At pH 4, degradation was relatively low (58% for CPF and 61.3% for IMD) due to limited hydroxyl radical generation and weaker adsorption on the catalyst surface. Efficiency increased steadily

Table 3. Comparative photocatalytic degradation efficiency of AgFeO₂ NC and other reported catalysts for CPF removal.

Sample	Synthesis method	Source of light	Pesticide	Time (min)	Parameters		Degradation rate (%)	Ref
					m (mg)	C (ppm)		
SPION@SiO ₂ @ TiO ₂	Chemical co-precipitation	UV-Visible	CPF	120 h	1 g/mL	50	95.7	(Herrera et al., 2024)
TiO ₂	Multi-step incipient wetness impregnation	UV-Visible	CPF	120 h	1 g/mL	50	52.3	(Herrera et al., 2024)
Cu_ TiO ₂ nanostructure	Electrochemical anodization	UV-Visible	IMD	60	0.8 M	25	45	(Čížmar et al., 2021)
C, N- TiO ₂ NPs	Sol-gel	UV-Visible	CPF	60	120	8	90	(Adanan et al., 2025)
TiO ₂ NPs	Green synthesis	Sun light	CPF	90	5	5	81	Present study
			IMD				83.5	
			CPF				95.6	
			IMD				97.3	
TiO ₂ /PHEMA NC								

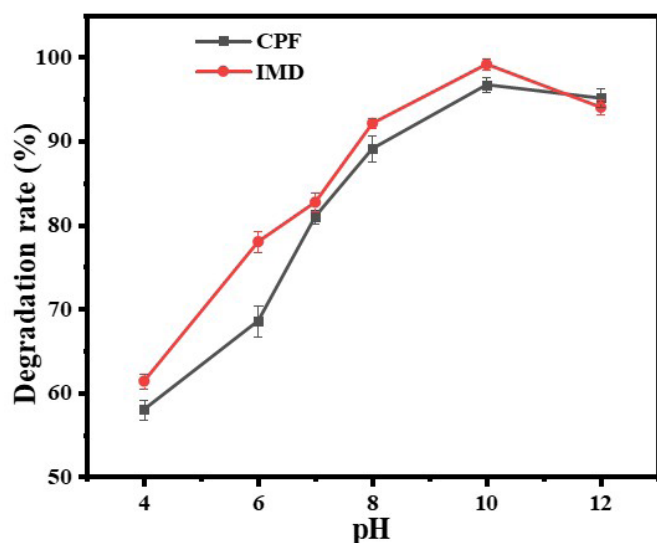


Fig. 7. Effect of pH on the photodegradation efficiency of CPF and IMD using TiO₂/PHEMA NC.

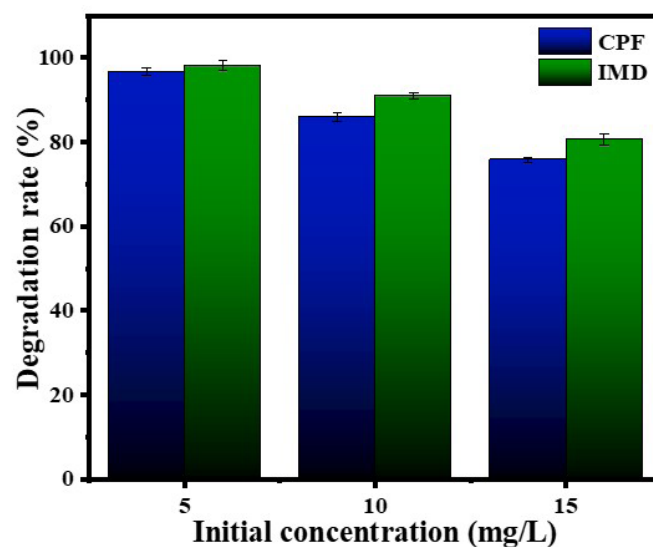


Fig. 8. Influence of initial concentration on CPF and IMD degradation by TiO₂/PHEMA NC.

with alkalinity, reaching 89.1% (CPF) and 92.1% (IMD) at pH 8 and peaking at 96.7% and 99.1%, respectively, at pH 10. The improvement is attributed to the higher availability of OH⁻ ions, which facilitate ·OH radical formation and accelerate photocatalytic oxidation (Nekooie et al., 2021). A slight decline beyond pH 10 (95.1% for CPF and 94.0% for IMD at pH 12) suggests that excess OH⁻ may act as radical scavengers, reducing activity. Notably, IMD consistently degraded more efficiently than CPF across the entire pH range, indicating greater susceptibility to photocatalytic attack. These findings confirm that alkaline conditions, particularly pH 10, are optimal for maximizing the photocatalytic efficiency of the TiO₂/PHEMA NC.

3.7.2. Effect of CPF and IMD initial concentration

The influence of initial pesticide concentration on the photocatalytic efficiency of the TiO₂/PHEMA NC (Fig. 8). At 5 mg L⁻¹, degradation reached 96.7% for CPF and 98.1% for IMD, demonstrating the high activity of the NC under dilute conditions. Increasing the concentration to 10 and 15 mg L⁻¹ led to progressive declines in efficiency, reaching 86% and 75.7% for CPF and 91% and 80.7% for IMD, respectively. This decrease is attributed to the saturation of active surface sites and reduced photon penetration at higher pollutant loads, which limit the generation of reactive oxygen species (Farahbakhsh et al., 2022). The consistently higher degradation of IMD compared to CPF suggests a greater susceptibility of IMD to photocatalytic oxidation, likely due to its molecular structure. These results confirm that the NC is highly effective at low-to-moderate concentrations, but efficiency decreases at higher pollutant levels due to kinetic and optical constraints.

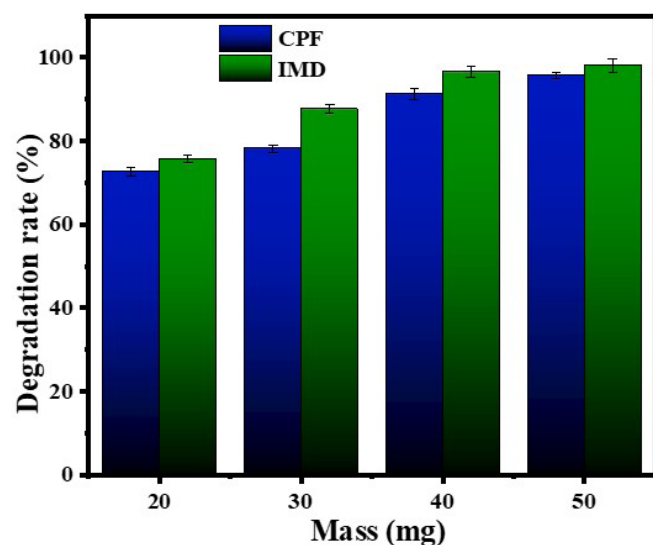


Fig. 9. Effect of photocatalyst amount for degradation of CPF and IMD using TiO₂/PHEMA NC.

3.7.3. The effect of photocatalyst dose

The effect of catalyst dosage on the photocatalytic degradation of CPF and IMD using the TiO₂/PHEMA NC has been shown in Fig. 9. At a catalyst mass of 20 mg, degradation efficiencies were relatively

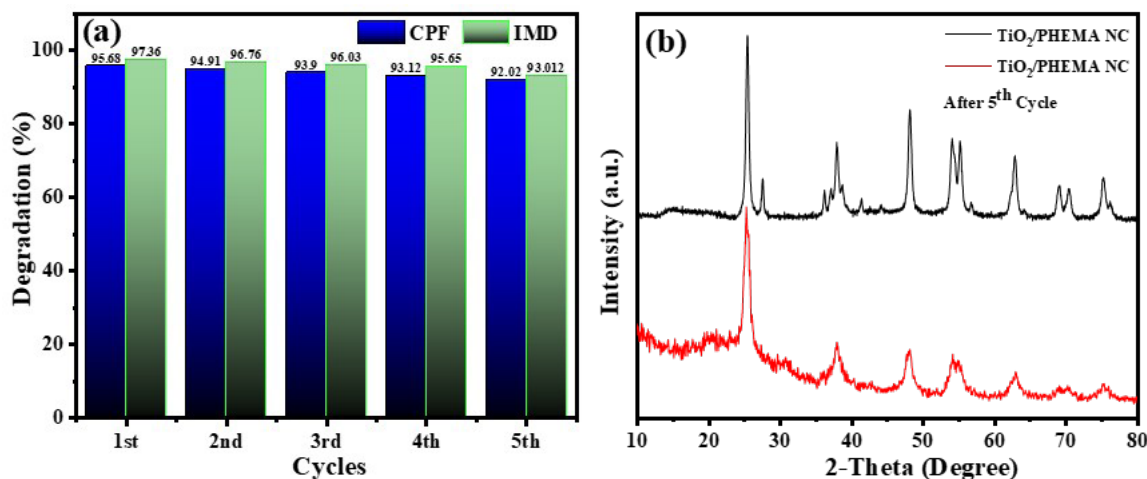


Fig. 10. (a) Reusability of TiO₂/PHEMA NC for CPF and IMD degradation over five cycles. (b) XRD patterns before and after cycling.

low, with 72.7% for CPF and 75.7% for IMD, reflecting the limited number of available active sites for pollutant adsorption and radical generation. Increasing the mass to 30 and 40 mg significantly enhanced degradation, achieving 78.1% and 91.2% for CPF and 87.6% and 96.6% for IMD, respectively, due to the greater surface area and higher density of active sites, which facilitated more efficient light absorption and the formation of reactive oxygen species. The maximum efficiency was obtained at 50 mg, with 95.7% CPF and 98.1% IMD degradation, indicating that beyond this dosage, the catalyst provides sufficient active surface to ensure nearly complete removal of the pesticides. These results demonstrate that photocatalytic efficiency strongly depends on catalyst loading, with optimal performance achieved when the mass provides sufficient active sites without introducing significant light scattering or shielding effects.

3.8. Reusability results

The recycling performance of the TiO₂/PHEMA NC has been shown in Fig. 10a. The photocatalyst maintained high degradation efficiencies for both CPF and IMD over five successive runs, with only a marginal decline observed. In the fifth run of the first cycle, efficiency decreased for CPF from 95.68% to 92.02%, while IMD degradation declined from 97.36% to 93.01%. The slight reduction in activity may be attributed to partial surface fouling by intermediate products or minor catalyst loss during recovery steps. Nevertheless, the photocatalyst consistently retained more than 92% efficiency even after the fifth cycle, demonstrating excellent stability, structural robustness, and reusability. These results confirm that the TiO₂/PHEMA NC is a durable and reliable photocatalyst for the repeated degradation of a pesticide under solar irradiation. XRD analysis before and after five photocatalytic cycles (Fig. 10b) further supports this conclusion. The fresh TiO₂/PHEMA NC displayed reflections of both anatase and rutile phases. However, after repeated use, the anatase peaks remained dominant while the weaker rutile signals at 27.6° and 36.2° were no longer detected. This suggests a gradual suppression of the rutile contribution, possibly due to preferential surface modification or structural reorganization under irradiation (Adanan *et al.*, 2025). Notably, the persistence of the anatase framework without new phases or amorphization demonstrates that the NC retains its essential crystalline integrity, which aligns with its sustained photocatalytic performance across multiple cycles.

3.9. Mechanism of photocatalytic activity

The photocatalytic degradation of CPF and IMD using TiO₂ NPs and TiO₂/PHEMA NC under sunlight irradiation can be rationalized based on the fundamental semiconductor photocatalysis pathway, as schematically illustrated in Fig. 11. Upon exposure to solar photons with energy equal to or greater than the band gap of TiO₂ (3.2 eV for pristine TiO₂, reduced to ~2.6 eV for TiO₂/PHEMA NC), electrons

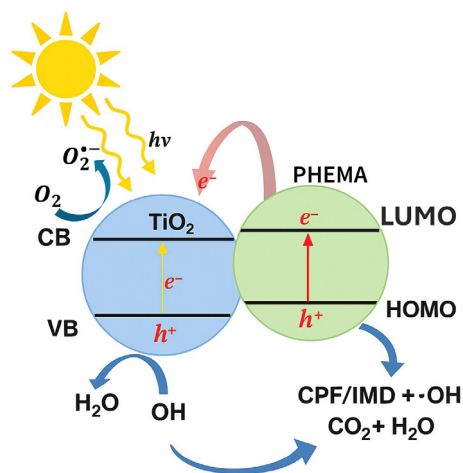
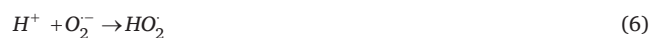


Fig. 11. Proposed photocatalytic degradation mechanism of CPF and IMD over TiO₂/PHEMA NC under sunlight irradiation.

(e⁻) in the valence band (VB) are excited to the conduction band (CB), leaving behind positively charged holes (h⁺) (Eq. 4):



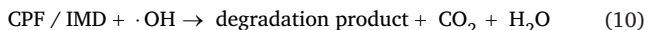
In the TiO₂/PHEMA NC, interfacial interactions between PHEMA functional groups and TiO₂ surface sites facilitate more efficient separation of these charge carriers, reducing recombination losses. The photoexcited electrons can migrate to the TiO₂ surface and react with dissolved molecular oxygen to form superoxide radicals (O₂⁻) (Eq. 5), which may undergo subsequent protonation and transformation into hydroperoxyl radicals (·HO₂) and eventually hydroxyl radicals (·OH) (Nekooie *et al.*, 2021) (Eqs. 6-8):



Meanwhile, photogenerated holes (h⁺) in the VB can directly oxidize water molecules or surface hydroxyl groups to produce additional hydroxyl radicals (Eq. 9):



These radicals ($\cdot OH$, $\cdot O_2$) are highly oxidative and non-selectively attack CPF and IMD molecules, initiating oxidative degradation via successive dechlorination, dealkylation, ring-opening, and eventual mineralization into CO_2 , H_2O , and other innocuous species (Adanan *et al.*, 2025).



The enhanced photocatalytic performance of the TiO_2 /PHEMA NC arises from synergistic effects: (i) extended light absorption due to bandgap narrowing, (ii) efficient charge separation at the TiO_2 -PHEMA interface via HOMO-LUMO alignment, and (iii) improved surface reactivity and dispersion, as evidenced by TEM, FTIR, and UV-Vis analyses.

4. Conclusions

This work introduces a novel TiO_2 /PHEMA NC as an efficient photocatalyst for the sunlight-driven degradation of CPF and IMD, two persistent and hazardous pesticides. Structural and optical analyses confirmed successful hybridization, with reduced bandgap energy, improved NP dispersion, and enhanced thermal and morphological stability. The NC outperformed pristine TiO_2 in degradation efficiency, kinetic rate, and operational stability, driven by its enhanced light absorption and effective charge separation facilitated by the PHEMA matrix. Photocatalytic performance was optimized by tuning pH, pollutant concentration, and catalyst loading, with alkaline conditions (pH 10) yielding the highest degradation rates. Moreover, the catalyst exhibited excellent reusability over five cycles with minimal loss in activity, underscoring its practical viability. The results establish TiO_2 /PHEMA as a robust and recyclable platform for pesticide remediation under natural sunlight, offering a green and scalable strategy for mitigating agrochemical pollution in aquatic environments. This study was conducted under controlled outdoor-simulated conditions; thus, validation in natural water matrices with co-existing contaminants is essential for real-world applicability. The absence of Brunauer-Emmett-Teller (BET) surface analysis also remains a limitation. Future work will address textural characterization, degradation pathway identification (LC-MS), testing in real wastewater, and pilot-scale synthesis.

CRedit authorship contribution statement

Zarah Alqarni: Conceptualization, data curation, formal analysis, funding acquisition, investigation, methodology, project administration, resources, software, supervision, validation, visualization, writing – original draft, writing – review & editing; conceptualization, data curation, methodology, resources, visualization, writing – original draft, writing – review & editing.

Declaration of competing interest

The authors declare that they have no competing financial interests or personal relationships that could have influenced the work presented in this paper.

Declaration of generative AI and AI-assisted technologies in the writing process

The authors confirm that there was no use of artificial intelligence (AI)-assisted technology for assisting in the writing or editing of the manuscript, and no images were manipulated using AI.

References

Adanan, N.A., Mohamad Idris, N.H., Lee, H.L., 2025. Carbon, nitrogen co-doped TiO_2 nanoparticles via sol-gel route: An approach for chlorpyrifos degradation. *Desal Water Treat* 321, 100935. <https://doi.org/10.1016/j.dwt.2024.100935>

- Akbari Shorgoli, A., Shokri, M., 2017. Photocatalytic degradation of imidacloprid pesticide in aqueous solution by TiO_2 nanoparticles immobilized on the glass plate. *Chem Eng Commun* 204, 1061-1069. <https://doi.org/10.1080/00986445.2017.1337005>
- Alamgir, M., Mallick, A., Nayak, G.C., 2021. Mechanical and thermal behavior of PHEMA and PHEMA nanocomposites targeting for dental materials. *Appl Nanosci* 11, 1257-1265. <https://doi.org/10.1007/s13204-021-01767-x>
- Alamgir, M., Nayak, G.C., Mallick, A., Sahoo, S., 2021. Effects of TiO_2 and GO nanoparticles on the thermomechanical properties of bioactive poly-HEMA nanocomposites. *Iran Polym J* 30, 1089-1099. <https://doi.org/10.1007/s13726-021-00948-3>
- Alamgir, M., Shahabuddin, S., Mallick, A., Nayak, G.C., 2022. Processing of PHEMA/ TiO_2 based nanocomposites used as an excellent dental materials. *Mater Today: Proc* 62, 7088-7091. <https://doi.org/10.1016/j.matpr.2022.01.235>
- Althamthami, M., Guettaf Temam, E., Temam, H.B., Saad, R., Hasan, G.G., 2023. Improved photocatalytic activity under the sunlight of high transparent hydrophilic Bi-doped TiO_2 thin-films. *J Photochem Photobiol A: Chem* 443, 114818. <https://doi.org/10.1016/j.jphtchem.2023.114818>
- Althamthami, M., Ben, T.H., Temam, G., Saad, R., Barkat, H., Nezzal, H., 2023b. Cost-effective Sol-Gel process for TiO_2 film coating on glass substrates: photocatalytic activity and structural characterization. *AS-Proceedings* 1, 31-34.
- Bokuniaeva, A.O., Vorokh, A.S., 2019. Estimation of particle size using the Debye equation and the Scherrer formula for polyphasic TiO_2 powder. *J Phys: Conf Ser*, 1410, 12057. <https://doi.org/10.1088/1742-6596/1410/1/012057>
- Boral, P., Varma, A.K., Maity, S., 2021. Nitration of Jharia basin coals, India: A study of structural modifications by XRD and FTIR techniques. *Int J Coal Sci Technol* 8, 1034-1053. <https://doi.org/10.1007/s40789-021-00422-8>
- Carboué, Q., Fadlallah, S., Lopez, M., Allais, F., 2022. Progress in degradation behavior of most common types of functionalized polymers: A review. *Macromol Rapid Commun* 43, e2200254. <https://doi.org/10.1002/marc.202200254>
- Čizmar, T., Panžič, I., Capan, I., Gajović, A., 2021. Nanostructured TiO_2 photocatalyst modified with Cu for improved imidacloprid degradation. *Appl Surf Sci* 569, 151026. <https://doi.org/10.1016/j.apsusc.2021.151026>
- Conde-Avila, V., Ortega-Martínez, L.D., Loera, O., El Kassis, E.G., Dávila, J.G., Valenzuela, C.M., Armendáriz, B.P., 2021. Pesticides degradation by immobilized microorganisms. *Int J Environ Anal Chem* 101, 2975-3005. <https://doi.org/10.1080/03067319.2020.1715375>
- Cosgrove, S., Jefferson, B., Jarvis, P., 2019. Pesticide removal from drinking water sources by adsorption: A review. *Environ Technol Rev* 8, 1-24. <https://doi.org/10.1080/21622515.2019.1593514>
- Erol, İbrahim, Yurdakal, S., Demirelli, K., Gürler, Z., 2022. Preparation of PHEMA/ TiO_2 nanocomposites by combination of in-situ polymerization/hydrothermal method and determination of their thermal, swelling, biological and dielectric properties. *J Polym Res* 29. <https://doi.org/10.1007/s10965-022-03146-8>
- Farahbakhsh, S., Parvari, R., Zare, A., Mahdizadeh, H., Faizi, V., Saljooqi, A., 2022. Preparation of biochar based on grapefruit peel and magnetite decorated with cadmium sulfide nanoparticles for photocatalytic degradation of chlorpyrifos. *Diam Relat Mater* 126, 109130. <https://doi.org/10.1016/j.diamond.2022.109130>
- Ghamarpoor, R., Fallah, A., Jamshidi, M., 2023. Investigating the use of titanium dioxide (TiO_2) nanoparticles on the amount of protection against UV irradiation. *Sci Rep* 13, 9793. <https://doi.org/10.1038/s41598-023-37057-5>
- Gopanna, A., Mandapati, R.N., Thomas, S.P., Rajan, K., Chavali, M., 2019. Fourier transform infrared spectroscopy (FTIR), Raman spectroscopy and wide-angle X-ray scattering (WAXS) of polypropylene (PP)/cyclic olefin copolymer (COC) blends for qualitative and quantitative analysis. *Polym Bull* 76, 4259-4274. <https://doi.org/10.1007/s00289-018-2599-0>
- Herrera, W., Vera, J., Hermosilla, E., Diaz, M., Tortella, G.R., Dos Reis, R.A., Seabra, A.B., Diez, M.C., Rubilar, O., 2024. The catalytic role of superparamagnetic iron oxide nanoparticles as a support material for TiO_2 and ZnO on chlorpyrifos photodegradation in an aqueous solution. *Nanomaterials (Basel)* 14, 299. <https://doi.org/10.3390/nano14030299>
- Johannes, A.Z., Pingak, R.K., Bukit, M., 2020. Tauc plot software: Calculating energy gap values of organic materials based on ultraviolet-visible absorbance spectrum. In: *IOP Conference Series: Materials Science and Engineering*. IOP Publishing, p 12030
- Khairan, S.D., Shrivastava, V.S., 2019. Photocatalytic degradation of chlorpyrifos and methylene blue using α - Bi_2O_3 nanoparticles fabricated by sol-gel method. *SN Appl Sci* 1. <https://doi.org/10.1007/s42452-019-0761-4>
- Kumar, A., Choudhary, P., Kumar, A., Camargo, P.H.C., Krishnan, V., 2022. Recent advances in plasmonic photocatalysis based on TiO_2 and noble metal nanoparticles for energy conversion, environmental remediation, and organic synthesis. *Small* 18, e2101638. <https://doi.org/10.1002/sml.202101638>
- Kumar, P., Arshad, M., Gacem, A., Soni, S., Singh, S., Kumar, M., Yadav, V.K., Tariq, M., Kumar, R., Shah, D., Wanale, S.G., Al Mesfer, M.K.M., Bhutto, J.K., Yadav, K.K., 2023. Insight into the environmental fate, hazard, detection, and sustainable degradation technologies of chlorpyrifos—an organophosphorus pesticide. *Environ Sci Pollut Res* 30, 108347-108369. <https://doi.org/10.1007/s11356-023-30049-y>
- Leskovic, A., Petrović, S., 2023. Pesticide use and degradation strategies: Food safety, challenges and perspectives. *Foods* 12, 2709. <https://doi.org/10.3390/foods12142709>
- Lothenbach, B., Durdzinski, P., De Weerd, K., 2016. Thermogravimetric analysis. A Pract Guid to Microstruct Anal Cem Mater 1, 177-211.
- Ma, F., Chen, J.-B., Wu, X.-X., Zhou, Q., Sun, S.-Q., 2016. Rapid discrimination of Panax notoginseng of different grades by FT-IR and 2DCOS-IR. *J Mol Struct* 1124, 131-137.
- Madurai Ramakrishnan, V., Pitchaiya, S., Muthukumarasamy, N., Kvamme, K., Rajesh, G., Agilan, S., Pugazhendhi, A., Velauthapillai, D., 2020. Performance of TiO_2

- nanoparticles synthesized by microwave and solvothermal methods as photoanode in dye-sensitized solar cells (DSSC). *Int J Hydrogen Energy* 45, 27036-27046. <https://doi.org/10.1016/j.ijhydene.2020.07.018>
- Makreski, P., Todorov, J., Makrievski, V., Pejov, L., Jovanovski, G., 2018. Vibrational spectra of the rare-occurring complex hydrogen arsenate minerals pharmacolite, picroparmacolite, and vladimirite: Dominance of Raman over IR spectroscopy to discriminate arsenate and hydrogen arsenate units. *J Raman Spectrosc* 49, 747-763.
- Malik, A.Q., Tabasum, S., Rani, S., Lokhande, P., Singh, P.P., Mooney, J., Singh, J., Alberto, H.-A.C., Sharma, A., Aepuru, R., Kumar, D., 2023. Fluorescent CdS QDs modified with molecular imprinted polymer for the photodegradation of imidacloprid and buprofezin pesticides under visible light. *J Inorg Organomet Polym* 33, 3468-3484. <https://doi.org/10.1007/s10904-023-02753-2>
- Mohammed, H.A., Bouafia, A., Laouini, S.E., Laib, I., Salmi, C., Alharthi, F., Mena, F., 2025. PEG-modified NiFe₂O₄ nanocomposites: Synthesis, characterization, and multifunctional biomedical applications in antioxidant, anti-inflammatory, photoprotective, antiemolytic, and antibacterial therapies. *Applied Organomet Chemis* 39. <https://doi.org/10.1002/aoc.70212>
- Moradi, O., Madanpishheh, M.A., Moghaddas, M., 2021. Synthesis of GO/HEMA, GO/HEMA/ TiO₂, and GO/Fe₃O₄/HEMA as novel nanocomposites and their dye removal ability. *Adv Compos Hybrid Mater* 4, 1185-1204. <https://doi.org/10.1007/s42114-021-00353-7>
- Motaung, T.E., 2020. Chloronicotinic insecticide imidacloprid: Agricultural relevance, pitfalls and emerging opportunities. *Crop Prot* 131, 105097. <https://doi.org/10.1016/j.cropro.2020.105097>
- Nahas, E.O., Furtado, G.F., Lopes, M.S., Silva, E.K., 2025. From emulsions to films: The role of polysaccharide matrices in essential oil retention within active packaging films. *Foods* 14, 1501. <https://doi.org/10.3390/foods14091501>
- Nandhini, A.R., Harshiny, M., Gummadi, S.N., 2021. Chlorpyrifos in environment and food: A critical review of detection methods and degradation pathways. *Environ Sci Process Impacts* 23, 1255-1277. <https://doi.org/10.1039/d1em00178g>
- Narayanan, N., Gupta, S., Gajbhiye, V.T., 2020. Decontamination of pesticide industrial effluent by adsorption-coagulation-flocculation process using biopolymer-nanoorganoclay composite. *Int J Environ Sci Technol* 17, 4775-4786. <https://doi.org/10.1007/s13762-020-02785-y>
- Nekooie, R., Shamspur, T., Mostafavi, A., 2021. Novel CuO/ TiO₂/PANI nanocomposite: Preparation and photocatalytic investigation for chlorpyrifos degradation in water under visible light irradiation. *J Photochem Photobiol A Chem* 407, 113038. <https://doi.org/10.1016/j.jphotochem.2020.113038>
- Nezzal, H., Rahmane, S., Temam, E.G., Al-Abri, M., Kyaw, H.H., Gasmii, B., Althamthami, M., Ben Temam, H., Hu, J., 2025. Photo-deposition of AgO thin films on TiO₂ substrate for (P-n) heterojunction applications: Considering the degree of contamination. *J Alloys Compd* 1010, 177331. <https://doi.org/10.1016/j.jallcom.2024.177331>
- Qutub, N., Singh, P., Sabir, S., Sagadevan, S., Oh, W.C., 2022. Enhanced photocatalytic degradation of acid blue dye using CdS/ TiO₂ nanocomposite. *Sci Rep* 12, 5759. <https://doi.org/10.1038/s41598-022-09479-0>
- Racovita, A.D., 2022. Titanium dioxide: Structure, impact, and toxicity. *Int J Environ Res Public Health* 19, 5681. <https://doi.org/10.3390/ijerph19095681>
- Rahimli, A., Musayeva, N., 2025. Tuning optical and structural properties of polystyrene nanocomposites with rutile TiO₂ nanoparticles. *Compos Interfaces* 32, 1123-1137. <https://doi.org/10.1080/09276440.2025.2457924>
- Saljooqi, A., Shamspur, T., Mostafavi, A., 2021. Synthesis and photocatalytic activity of porous ZnO stabilized by TiO₂ and Fe₃O₄ nanoparticles: Investigation of pesticide degradation reaction in water treatment. *Environ Sci Pollut Res Int* 28, 9146-9156. <https://doi.org/10.1007/s11356-020-11122-2>
- Salmi, C., Souhaila, M., Salah Eddine, L., Mohammed, H.A.M., Hasan, G.G., Mahboub, M.S., 2024. Biosynthesis of Mn₃O₄/PVP nanocomposite for enhanced photocatalytic degradation of organic dyes under sunlight irradiation. *J Clust Sci* 35, 201-215. <https://doi.org/10.1007/s10876-023-02475-y>
- Salmi, C., Zelca, Z., Laouini, S.E., Meneceur, S., Mohammed, H.A., Abdullah, J.A.A., Abdullah, M.M.S., 2025. Gallic acid assisted synthesis of novel CuO/Ni/Fe₃O₄ nanocomposite for catalytic CO₂ methanation and photocatalytic hydrogen generation. *J Sol-Gel Sci Technol* 113, 670-682. <https://doi.org/10.1007/s10971-024-06608-1>
- Shejale, K.P., Krishnapriya, R., Patil, H., Laishram, D., Rawal, P., Sharma, R.K., 2021. Recent advances in ultra-low temperature (sub-zero to 100° C) synthesis, mechanism and applications of titania (TiO₂) nanoparticles. *Mater Adv* 2, 7502-7529. <https://doi.org/10.1039/D1MA00942G>
- Tan, N.P.B., Lee, C.H., Li, P., 2016. Green synthesis of smart metal/polymer nanocomposite particles and their tuneable catalytic activities. *Polymers* (Basel) 8, 105. <https://doi.org/10.3390/polym8040105>
- Tiwari, A., Dhoble, S.J., 2016. Stabilization of ZnS nanoparticles by polymeric matrices: Syntheses, optical properties and recent applications. *RSC Adv* 6, 64400-64420. <https://doi.org/10.1039/c6ra13108e>
- Toledo, L., Racine, L., Pérez, V., Henríquez, J.P., Auzely-Velty, R., Urbano, B.F., 2018. Physical nanocomposite hydrogels filled with low concentrations of TiO₂ nanoparticles: Swelling, networks parameters and cell retention studies. *Mater Sci Eng C Mater Biol Appl* 92, 769-778. <https://doi.org/10.1016/j.msec.2018.07.024>
- Ussia, M., Di Mauro, A., Mecca, T., Fregonese, D., Gattazzo, C., Iwuoha, E., Righettoni, M., Caccamo, M.T., 2018. ZnO- PHEMA nanocomposites: an ecofriendly and reusable material for water remediation. *ACS Appl Mater Interfaces* 10, 40100-40110. <https://doi.org/10.1021/acsami.8b16315>
- Wu, H., Li, L., Wang, S., Zhu, N., Li, Z., Zhao, L., Wang, Y., 2023. Recent advances of semiconductor photocatalysis for water pollutant treatment: Mechanisms, materials and applications. *Phys Chem Chem Phys* 25, 25899-25924. <https://doi.org/10.1039/d3cp03391k>
- Yoloğlu, E., Uçkun, M., Alkan Uçkun, A., Barım Öz, Özden, 2025. Biochemical responses of crayfish exposed to imidacloprid: Assessment of oxidative stress, osmoregulatory response and neurotoxicity. *Chem Ecol* 41, 50-68. <https://doi.org/10.1080/02757540.2024.2402294>
- Zhang, X., Sun, J., 2020. Synthesis, Characterization, and Properties of Sulfonated Chitosan for Protein Adsorption. *Int J Polym Sci* 2020, 1-10. <https://doi.org/10.1155/2020/9876408>
- Zhou, W., Li, M., Achal, V., 2025. A comprehensive review on environmental and human health impacts of chemical pesticide usage. *Emerg Contam* 11, 100410. <https://doi.org/10.1016/j.emcon.2024.100410>